

Search for low lying dipole strength in the neutron rich nucleus ^{26}Ne

J. Gibelin^{a,b*}, D. Beaumel^a, T. Motobayashi^c, N. Aoi^c, H. Baba^c, Y. Blumenfeld^a, Z. Elekes^d, S. Fortier^a, N. Frascaria^a, N. Fukuda^c, T. Gomi^c, K. Ishikawa^e, Y. Kondo^e, T. Kubo^c, V. Lima^a, T. Nakamura^e, A. Saito^f, Y. Satou^e, E. Takeshita^b, S. Takeuchi^c, T. Teranishi^f, Y. Togano^b, A. M. Vinodkumar^e, Y. Yanagisawa^c, K. Yoshida^c

^aInstitut de Physique Nucléaire, IN₂P₃-CNRS, F-91406 Orsay, France

^bDepartment of Physics, Rikkyo University, 3-34-1 Nishi-Ikebukuro, Toshima, Tokyo 171-8501, Japan

^cRIKEN (The Institute of Physical and Chemical Research), 2-1 Hirosawa, Wako, Saitama 351-0198, Japan

^dInstitute of Nuclear Research of the Hungarian Academy of Sciences, PO Box 51, H-4001 Debrecen, Hungary

^eDepartment of Physics, Tokyo Institute of Technology, Tokyo 152-8551, Japan

^fCentre for Nuclear Study, University of Tokyo, RIKEN Campus, 2-1 Hirosawa, Wako, Saitama 351-0198, Japan

Coulomb excitation of the exotic neutron-rich nucleus ^{26}Ne on a ^{nat}Pb target was measured at 58 A.MeV in order to search for low-lying E1 strength above the neutron emission threshold. Data were also taken on an ^{nat}Al target to estimate the nuclear contribution. The radioactive beam was produced by fragmentation of a 95 A.MeV ^{40}Ar beam delivered by the RIKEN Research Facility. The set-up included a NaI gamma-ray array, a charged fragment hodoscope and a neutron wall. Using the invariant mass method in the $^{25}\text{Ne}+n$ channel, we observe a sizable amount of E1 strength between 6 and 10 MeV. The reconstructed ^{26}Ne angular distribution confirms its E1 nature. A reduced dipole transition probability of $B(E1) = 0.49 \pm 0.16 \text{ e}^2\text{fm}^2$ is deduced. For the first time, the decay pattern of low-lying strength in a neutron-rich nucleus is obtained. The results are discussed in terms of a pygmy resonance centered around 9 MeV.

1. Introduction

Giant Resonances are a general feature of nuclei and their properties give us a handle on the macroscopic and microscopic behavior of nuclear matter. These modes have been extensively studied in stable nuclei over the last 50 years and the recent inception of Radioactive Ion Beam facilities opens the opportunity to extend these investigations to

*present address: Lawrence Berkeley National Laboratory, CA 94720 Berkeley, USA

exotic nuclei. Far from stability new modes are expected to appear. In particular, the dipole response of neutron-rich nuclei may exhibit strength at energies lower than the standard Giant Dipole Resonance (GDR) often depicted as the oscillation of a deeply bound core against a neutron skin giving rise to a so-called pygmy resonance. Recent studies on Oxygen [1] and Tin [2] isotopes have given the first experimental indications for such an effect, while at the same time calling into question its nature.

The theoretical approach is often based on mean field calculations. Relativistic random phase approximation (RRPA) and quasi-particle RRPA (QRRPA) calculations have been carried out by Cao and Ma in ^{26}Ne [3] which predict that below 10 MeV excitation energy, almost 5% of the Thomas-Reiche-Kuhn (TRK) energy weighted sum rule is exhausted by strength centered around 8 MeV. This region of energy is located between the one neutron and the two neutron emission thresholds. Thus, in order to investigate this prediction, we performed Coulomb excitation of ^{26}Ne at intermediate energies on a lead target and used the invariant mass method to reconstruct the B(E1) strength from the $^{26}\text{Ne} \rightarrow ^{25}\text{Ne}^* + n$ reaction.

2. Experimental details

The experiment was performed at the RIKEN Accelerator Research Facility. A secondary ^{26}Ne beam was produced through fragmentation of a 95 A.MeV ^{40}Ar primary beam on a 2-mm-thick ^9Be target. The ^{26}Ne was separated by the RIKEN Projectile Fragment Separator (RIPS) [4]. Particle identification was unambiguously performed by means of the time-of-flight (TOF) and the purity was 80%. The ^{26}Ne beam of intensity $\sim 5.10^3$ pps and incident energy 58 A.MeV, was tracked with two parallel-plate avalanche counters providing incident angle and hit position onto the target. It then impinged alternatively on a 230 mg/cm² ^{nat}Pb and a 130 mg/cm² ^{nat}Al target. Data obtained with aluminum target are used in the following to estimate the contribution of nuclear excitation to the data.

The outgoing charged fragments were measured using a set of telescopes placed at 1.2 m downstream of the target. They consisted of two layers (X and Y) of 500 μm silicon strip detectors (SSD) with 5 mm strips which provided an total energy resolution of 1.5 MeV (FWHM). The last layer used 3-mm-thick Si(Li) from the charged-particle detector MUST [5], provided a 9 MeV (FWHM) resolution on the remaining energy (E). Unambiguous mass and charge identification of all projectile like fragments was obtained using the E- Δ E method.

In-beam gamma rays were detected using a 4 π -gamma-detector, DALI2 [6], which consists of 152 NaI detectors placed around the target. For 1.3 MeV gamma-rays, its measured efficiency is approximately 15% with an energy resolution of 7% (FWHM). The Doppler corrected gamma energy distribution obtained in coincidence with the ^{25}Ne isotope allows us to identify the gamma decay from the adopted 1702.7(7) keV and 3316.4(11) keV excited states. In addition we observed a 2063 ± 67 keV gamma-ray which we related to the 2030 ± 50 keV excited state, only seen up to now by transfer reaction [7].

The hodoscope for neutron detection was an array of 4 layers of 29 plastic rods each, placed 3.5 m downstream of the target. Each layer was composed of 13 [2.1 m \times 6 \times 6 cm²] and 16 [1.1 m \times 6 \times 6 cm²] rods, arranged in a shape of a cross. Its total intrinsic efficiency

for the detection of one 60 MeV neutron was calculated to be $\sim 25\%$. Finally 29 thin plastic rods covered the front face of the wall in order to veto charged particles as well as to provide an active beam stopper. The neutron position is determined with an error of ± 3 cm and the energy, from TOF information, with a 2.5 MeV (FWHM) resolution for the neutrons of interest.

3. Results

We have performed a simulation of the experimental setup using the Geant 3 package [8]. In order to check the reliability of the analysis, we built the elastic scattering angular distribution of ^{26}Ne on ^{nat}Pb at 55 A.MeV. It is in good agreement with a DWBA calculation based on a $^{20}\text{Ne}+^{208}\text{Pb}$ at 40 A.MeV optical potential from [9]. We empirically generated optical potential parameters for the $^{26}\text{Ne}+^{27}\text{Al}$ reaction and tested them by comparing with the experimental elastic scattering.

Using the invariant mass method, the excitation energy of an unbound state in the nucleus ^AX decaying to a state in ^{A-1}X can be expressed by: $E^* = E_{\text{rel}} + S_n + \sum_i E_{\gamma_i}$, where E_{rel} is the relative energy between neutron and ^{A-1}X and S_n the one neutron emission threshold. The gamma detection efficiency was not high enough to apply an event-by-event reconstruction technique. To extract the excitation energy spectrum, we hence used a method based on adequate subtraction of relative energy spectra built for these two kind of event.

The method can be illustrated in the schematic case where the daughter nucleus ^{A-1}X has only one excited state below its neutron threshold. The excitation energy spectrum can be decomposed in the sum of two contributions: the decay of ^AX to the ground-state (gs) of ^{A-1}X and the decay of ^AX to the excited state (I) of ^{A-1}X .

The first contribution can be obtained by subtracting from the inclusive relative energy spectrum $[E_{\text{rel}}(^{A-1}\text{X}, n)]$ the relative spectrum of gamma-coincidence events $[E_{\text{rel}}(^{A-1}\text{X}, n)|_{\gamma}]$ divided by the gamma detection efficiency ϵ , and shifted “ \leftrightarrow ” by the one neutron emission threshold S_n *i.e.*: $[E^*]^{gs} = [E_{\text{rel}}(^{A-1}\text{X}, n)] - [E_{\text{rel}}(^{A-1}\text{X}, n)|_{\gamma}] / \epsilon \leftrightarrow S_n$.

The second contribution is simply the relative energy spectrum of gamma-coincidence events shifted by the gamma energy: $[E^*]^{(I)} = [E_{\text{rel}}(^{A-1}\text{X}, n)|_{\gamma}] / \epsilon \leftrightarrow S_n \leftrightarrow E_{\gamma}$. Finally, the excitation energy spectrum for the $^{25}\text{Ne}+n$ decay channel is given by: $[E^*] = [E^*]^{gs} + [E^*]^{(I)}$. The method was tested by simulation in this schematic case, and also in the realistic case taking into account the experimental decay scheme of ^{25}Ne .

The excitation energy spectra reconstructed for the $^{25}\text{Ne}+n$ decay channel obtained with the ^{nat}Pb and ^{nat}Al targets are represented on Fig. 1. Note that above $S_{2n} = 9.8$ MeV, the decay of ^{26}Ne is expected to occur mainly by 2 neutron emission. Between 8 and 10 MeV, a sizable amount of cross-section is observed for both targets. In intermediate energy inelastic scattering with a heavy target such as ^{nat}Pb , the Coulomb dominance of the E1 excitation is well-known. The contribution of possible E2 excitation to the spectrum obtained with the lead target has — in a first step — been determined using data taken with the aluminum target and the coupled channels ECIS 97 [10] code. Assuming simple collective vibration mode with equal nuclear and Coulomb deformation lengths, the E2 deformation parameters were extracted from the measured cross-section with the ^{nat}Al target ($\sigma_{\text{Al}} = 9.1 \pm 2.3$ mb). The $L = 2$ cross section in lead was then calculated using

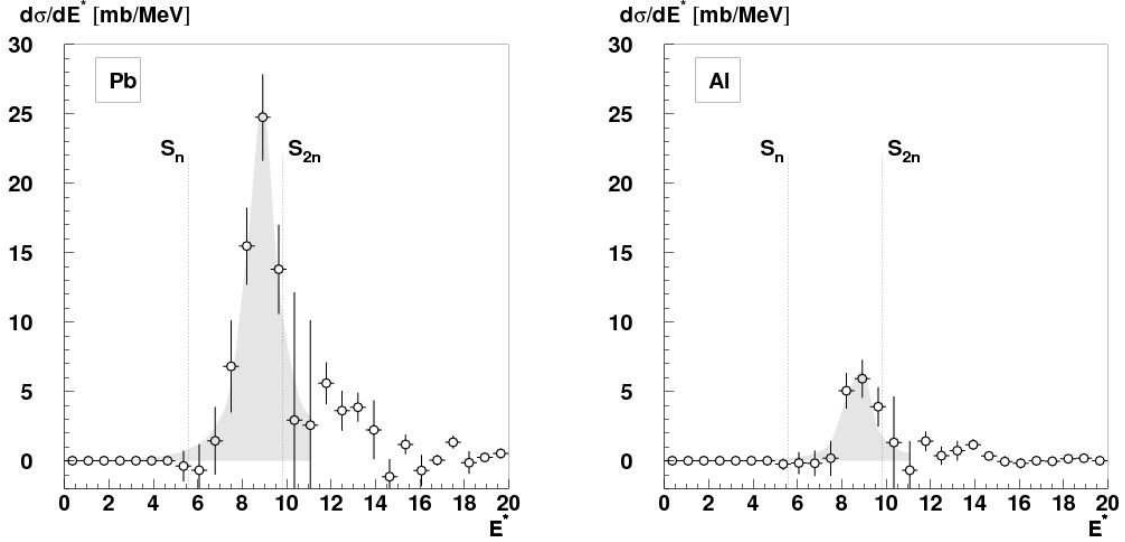


Figure 1. **Left:** Excitation energy distribution in ^{26}Ne in the ^{nat}Pb target. The shaded area is a tentative Lorentzian fit. **Right:** Same as previous but for the ^{nat}Al target.

the deformation lengths extracted in the previous step. We obtained $\sigma_{\text{Pb}}^{L=2} = 17.9 \pm 4.3$ mb. After subtraction of the $L = 2$ contribution, the resulting $\sigma_{\text{Pb}}^{L=1} = 48.5 \pm 4.8$ mb cross section corresponds, using ECIS 97, to a Coulomb deformation parameter of $\beta_C = 0.087 \pm 0.05$ which led to a $B(E1) = 0.55 \pm 0.05$ e 2 fm 2 *via* the relation $B(E1; 0^+ \rightarrow 1^-) = \left(\frac{3}{4\pi} Z_p e R_C \beta_C^{L=1}\right)^2$ with R_C the Coulomb radius. This value of reduced transition probability correspond to $5.5 \pm 0.6\%$ of the Thomas-Reiche-Kuhn energy weighted sum rule for an excitation energy of 9 MeV. We estimate the error due to the choice of optical potential by performing the same analysis using now parameters from the $^{40}\text{Ar}+^{208}\text{Pb}$ reaction at 40 A.MeV [11]. We obtained $B(E1) = 0.60 \pm 0.06$ e 2 fm 4 *i.e.* $6.0 \pm 0.6\%$ of the TRK, in good agreement with the values previously extracted, which demonstrates that we are not strongly sensitive to the choice of the optical potential for the reaction on lead.

Due to the high granularity and the good resolution of the present setup, it is possible to reconstruct the scattering angular distribution for ^{26}Ne on the ^{nat}Pb target which is represented in Fig. 2. Hence, we have used a second method to extract the E1 excitation which relies on a multipole decomposition analysis of this angular distribution. The $L = 1$ and $L \geq 2$ angular distributions (dashed and dotted lines) were obtained from simulation based on ECIS 97 angular distribution calculated for $E^* = 9$ MeV. The data were fitted with a linear combination of the two distributions. The results of the fit give us $B(E1) = 0.49 \pm 0.16$ which corresponds to $4.9 \pm 1.6\%$ of the TRK, again for an excitation energy of 9 MeV. If we suppose now that the remaining part of the contribution is due to $L = 2$ excitation we can extracted a $B(E2 \uparrow) = 49 \pm 8$ e 2 fm 4 for this structure.

The two results from the two different methods are in agreement but since the multipole decomposition of the angular distribution relies only on the data from lead target, the

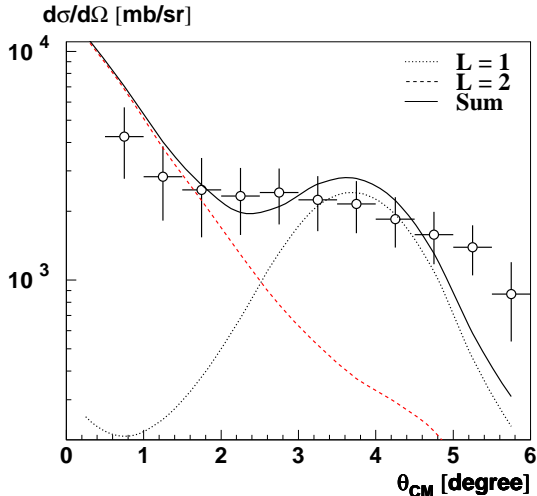


Figure 2. Result (solid line) of the multipole decomposition of the experimental angular distribution (circle) of the ^{26}Ne angular scattering onto lead target, by $L = 1$ (dashed line) and $L = 2$ -type (dotted line) distributions.

second value of $B(E1) = 0.49 \pm 0.16 \text{ e}^2\text{fm}^2$ will be retained. The results obtained from our experiment concerning the E1 transition are compared in the following to theoretical calculations.

4. Comparison with theory

In the introduction we already presented results from Cao and Ma [3]. Using the relativistic QRPA framework and the response function formalism they predicted a pygmy resonance centered around 8.4 MeV and which exhausts 4.5% of the TRK, which is close to our experimental values. Another calculation has been performed by Khan *et al.* [12]. It is based on effective SGII Skyrme interactions and is performed in the spherical QRPA framework. It predicts a redistribution of the strength at low energy centered around $E^* = 11.7 \text{ MeV}$ exhausting $\sim 5\%$ of the TRK. Two other preliminary calculations has been performed in the deformed QRPA framework using Gogny forces [13] and in the deformed relativistic QRPA framework [14]. Both predict a redistribution of the strength at low energy, centered around 10.7 MeV and 7.5 MeV respectively. The first calculation also predicts that only $\sim 1\%$ of the TRK should be exhausted. Preliminary shell-model calculations have also been performed by Nowacki *et al.* [15] who predict a state at 9.3 MeV exhausting $\sim 5\%$ of the TRK. All these theories agree on the presence of a 1^- structure a low excitation energy, compatible with our experimental result but they disagree on its nature: the amount of strength differs as well as as well as its collective or single particle nature.

5. Decay of pygmy resonances in ^{26}Ne

Our reconstruction method for the excitation energy allows us to extract for the first time data on the decay of pygmy resonance of neutron-rich nuclei. We present the experimental branching ratios towards the various states of ^{25}Ne in Tab. 1. The clear difference between the branching ratios obtained with lead and aluminum targets proves that states of different nature have been excited. For comparison, we also performed a statistical

Table 1

Experimental branching ratio compared to statistical model for a given ^{26}Ne transition multipolarity to a given excited state in ^{25}Ne compared to experiment.

Final ^{25}Ne state		Experiment		Statistical decay		
Label	J^Π	Pb	Al	$L = 1$	$L = 2$	$L = 3$
(gs)	$1/2^+$	$5_{-5}^{+17}\%$	$< 10\%$	40%	28%	22%
(I)	$5/2^+ + 3/2^+$	$66\% \pm 15\%$	$95_{-15}^{+5}\%$	55%	67%	75%
(II)	$3/2^-$	$35\% \pm 9\%$	$5_{-5}^{+6}\%$	5%	4%	3%

decay calculation for $L = 1, 2, 3$ states using the CASCADE code[16], assuming spins and parities of ^{25}Ne states as listed in Tab. 1. It clearly shows that the decay is not statistical, which is not surprising for a light nucleus. No predictions of the direct decay of pygmy states yet exist from the previously mentioned microscopic models. Future comparisons with our data should be a strong test for these models.

6. Conclusion

We performed the Coulomb excitation of ^{26}Ne in order to measure its low lying dipole strength below 10 MeV excitation energy, using the invariant mass method. We extract an E1 strength value of $B(E1) = 0.49 \pm 0.16 \text{ e}^2\text{fm}^2$ between the one- and the two-neutron emission threshold as well as the corresponding decay pattern. Our results are compatible with various theoretical predictions. Future comparison of the extracted decay pattern with theoretical models may allow us to elucidate whether the strength is of single particle nature or rather due to a collective pygmy resonance.

REFERENCES

1. A. Leistenschneider, et al., Phys. Rev. Lett. 86 (2001) 5442.
2. P. Adrich, et al., Phys. Rev. Lett. 95 (2005) 132501.
3. L.-G. Cao, Z.-Y. Ma, Phys. Rev. C 71 (2005) 034305.
4. T. Kubo, et al., Nucl. Ins. and Meth. B 70 (1992) 309.
5. Y. Blumenfeld, et al., Nucl. Ins. and Meth. A 421 (1999) 471.
6. S. Takeuchi, et al., RIKEN Accel. Prog. Rep. 36 (2002) 148.
7. R. H. Wilcox, et al., Phys. Rev. Lett. 30 (1973) 866.
8. R. Brun, et al., CERN DD/EE/84-1.
9. T. Suomijärvi, et al., Nucl. Phys. A 491 (1989) 314.
10. J. Raynal, ECIS-97, Unpublished.
11. T. Suomijärvi, et al., Nucl. Phys. A 509 (1990) 369.
12. E. Khan, et al., Private communication (2005).
13. S. Péru, et al., This proceedings (2006).
14. P. Ring, et al., This proceedings (2006).
15. F. Nowacki, et al., Private communication (2005).
16. F. Puhlhofer, Nucl. Phys. A 280 (1977) 267.